Mechanics of Advanced Composite Structures 9 (2022) 59 – 73
This is an Open Access paper licensed under the Creative Commons License CC-BY 4.0 license.
Semnan University

Mechanics of Advanced Composite Structures

journal homepage: http://MACS.journals.semnan.ac.ir

3D Numerical Simulation of Fibers Arrangement Effects on Thermal Conductivity of Polymer Matrix Composite

M. M. Peiravi, J. Alinejad *

Department of Mechanical Engineering, Sari Branch, Islamic Azad University, Sari, Iran

KEYWORDS

Different fibers arrangement;
Lattice Boltzmann method;
Polymer matrix composite;
Thermal conductivity.

ABSTRACT

This study investigated the effects of different arrangements of three-dimensional fibers on polymer matrix composite thermal conductivity under heat flux boundary conditions. The thermal lattice Boltzmann based on the D3Q7 (three dimensions and seven temperature vectors) method is utilized to illustrate the thermal conductivity in 7 cases of PMC with a different arrangement of 3D fibers. Nondimensional temperature fields, isothermals, nondimensional thermal conductivity coefficient, nondimensional mean, and local temperature in 7 cases of PMCs have been investigated. The non-dimensional thermal conductivity coefficient in each PMC has been analyzed to predict optimal levels of factors affecting this simulation to maximize and minimize the heat transfer rate. The results signified that nondimensional temperature field in a PMC with the arrangement of a fiber, triplet, and triangular perpendicular to heat flux had a greater rate than a PMC with the arrangement of fibers along the way heat flux. Also, the Maximum and minimum of nondimensional thermal conductivity coefficient were in PMC with the arrangement of triplet fibers perpendicular to heat flux, $(k_{x,c} = 1.017)$ and triangular fibers along the way heat flux, $(k_{x,f} = 0.809)$respectively.

1. Introduction

Polymer Matrix Composite (PMC) is a practical material made of polymer and a reinforcing phase untitled fiber. Inside the polymer, the fibers are arranged as unidirectional fibers, veil mat, chopped strands, and woven fabric. manufacturing methods of PMCs are popular is simple and low cost, as well as suitable strength. So, practical applications of PMCs are in industries such as secondary load-bearing aerospace structures, boat bodies, automotive parts. The presented paper attempted to investigate the effects of different arrangements of 3D fibers on polymer matrix composite thermal conductivity under heat flux boundary conditions with the Lattice Boltzmann Method (LBM). LBM has been evolving over the last two decades. The physics of microscopic processes is considered by simplifying kinetic models in LBM [1]. In this simulation, once streaming is done, new distribution components of Lattice nodes are calculated to obtain the updated macroscopic properties [2]. This method of calculating macroscopic values essentially differs from what is done in other traditional Computational Fluid Dynamic (CFD) methods. Algorithm simplicity, fully parallel computation, and easy implementation of complex boundary conditions are among the numerous superiorities of LBM [3]. Also, it is shown strong potential in simulating nonlinear mathematical-physical equations [4]. It should be noted that these models always deal with stability issues, and therefore in the last few years, several researches have been done to solve this problem, such as Two Relaxation Time (TRT) models and Multi Relaxation Time (MRT) model. Peiravi et al. [5] surveyed a 3D multi-phase nanofluid natural convection and radiation effect based on numerical and analytical simulation. Mal et al. [6] studied the effect of thermal conductivity and electrochemical properties of a composite solid polymer-based on polyvinyl alcohol matrix by the casting method. Torres et al. [7] analyzed the behavior of composite materials mixed with polymer and ceramic matrix. They surveyed the resistance of solid residuals against wet abrasive.

* Corresponding author. . Tel.: +98-11-33032891; Fax: +98-11-33033751
E-mail address: Alinejad_javad@iausari.ac.ir

DOI: 10.22075/macs.2022.21131.1291
Received 2020-08-17; Received in revised form 2021-11-15; Accepted 2022-01-01
© 2022 Published by Semnan University Press. All rights reserved.

Fois et al. [8] investigated heat transfer mechanisms in PMCs containing micro-encapsulated paraffin in latent energy storage systems. Ivosevic et al. [9] improved the resistance of thermally sprayed for the erosion and oxidation of PMCs with varying volume fractions of WC–Co. Cenna et al. [10] experimentally investigated wear mechanisms in composite materials subjected to friction by bulk solids. Roy et al. [11] analyzed four different composite materials with glass fibers against solid particle erosion. Shemelya et al. [12] studied the effect of graphite, silver, and carbon fiber geometry in an acrylonitrile butadiene styrene polymer matrix on the thermal conductivity. Han et al. [13] investigated the effect of filler incorporation and curing pressure on the thermal conductivity of carbon fiber PMC. Kim et al. [14] investigated the electrical and thermal effects of a silver flake PMC using a 3D resistor network model. Yamada et al. [15] surveyed the thermal conductivity of carbon fiber PMCs by Nanostructuring the interlaminar interface with carbon black on heat dissipation of aircraft. Alva et al. [16] presented thermal and electrical effects on boron nitride, zinc oxide, and silicon carbide ceramic nanofibers with polyvinyl butyral polymer matrix in PMC applications. Wang et al. [17] simulated the thermal reaction and erosion in glass fiber in PMCs subjected to a lightning strike. Moradi et al. [18] investigated the effect of thermal conductivity and open-hole size on mechanical characteristics of PMCs. Yu et al. [19] surveyed thermal conductivity and mechanical characteristics of carbon fiber in three-dimensional PMCs. Takenaka et al. [20] studied thermal characteristics of PMCs with negative thermal expansion materials in injection molding. Chen et al. [21] presented the electrical and thermal conductivity of PMC with graphene/aluminum nanofibers in electronic devices. Recently, Ouyang et al. [22] investigated the thermal conductivity of PMCs with network Al_2O_3 spheres fibers. Wang et al. [23] presented the electrical effect and high thermal conductivity of PMCs with polyamide 6/carbon nanofiber composites in braze welding technology. Shigang et al. [27] numerically investigated three dimensional thermal conductivity of Woven C/C composites from 300 to 2500 K. Lu et al. [28] numerically surveyed the elastic properties of three dimensional fiber composites with a wide range of fiber aspect ratios. Klein et al. [29] used a numerical homogenization approach in order to study the principal influence of key composite descriptors of fiber and particle reinforced PEEK on the homogenized heat conductivity. Karkri et al. [30] used a three-dimensional (3D) finite elements method for predicting the effective thermal conductivity (ETC) of a conductive hollow tube polymer composite. Liang et al. [31] presented a model for simulating the microscopic heat transfer processes in a wood-metal composite material. The model was developed by analyzing the microstructure of experimental samples comprising a melted alloy impregnated in a wood matrix. Karkri et al. [32] presented a numerical and experimental study of a composite material with conducting spheres embedded in a polymer matrix. Ejeh et al. [33] investigated the carbon fibers doped with nanoparticles of silicon carbide (CFSiC) and resin bonded glass fiber (RBGF). It was found that the results were distinctly different when compared with the CFRP laminate. CFSiC showed to exhibit an enhanced thermo-elastic behaviour, due to the high thermal stability of SiC nanoparticles in the composite. In the presented paper, the model is validated by comparing with analytical result [24]. Then nondimensional thermal conductivity characteristics and temperature field are investigated for different arrangement of 3D fibers in PMC under heat flux boundary condition.

2. Problem Definition

The effects of different arrangement of 3D fibers on the thermal conductivity of PMC under heat flux boundary condition is presented numerically. The conduction heat transfer characteristics are optimized with seven fibers and polymer matrix cases in a different arrangement. The boundary conditions for PMC under heat flux are illustrated in Fig. 1. The dimensions of each 3D enclosure are L×L×L. The present study investigated fibers effects on thermal profiles from the heat flux wall to the cold temperature wall. So, according to our research, these seven cases have the most critical effect on thermal conductivity.

Thermal conductivity coefficient in *i* direction for fiber and polymer matrix are $k_{1,i}$ and $k_{2,i} = k_{1,i}(T_1 - T_c/T_2 - T_c)$, respectively. Where T_1 and T_2 are unknown temperatures on the wall with constant heat flux for fiber and polymer matrix, respectively. The conduction heat transfer equation for the problem is represented in Eq. (1) [24]:

$$q = k\frac{\partial T}{\partial n} \quad (1)$$

where, k= (k_x, k_y, k_z) and n= (x, y, z).

3. Simulation Methodology

3.1. Lattice Boltzmann Method

The lattice Boltzmann method is a powerful numerical method for simulating thermal conductivity. This method has many advantages in comparing conventional CFD methods of calculating energy equations.

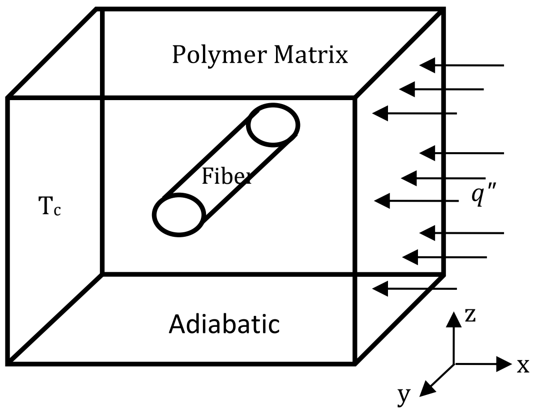

a) A fiber perpendicular to heat flux

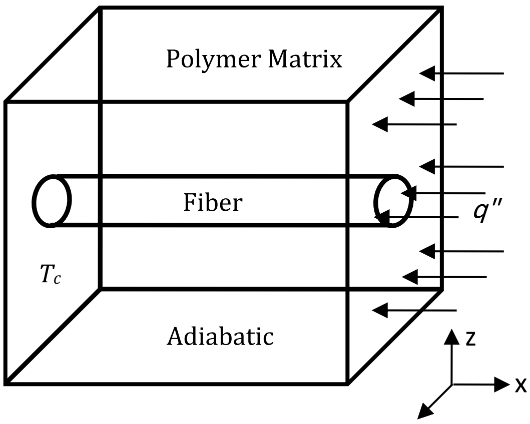

b) A fiber along the way heat flux

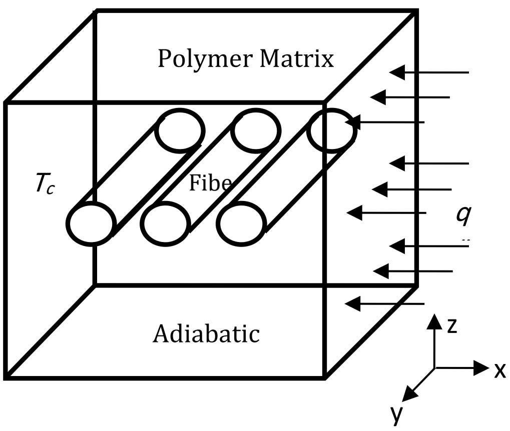

c) Triplet fibers perpendicular to heat flux

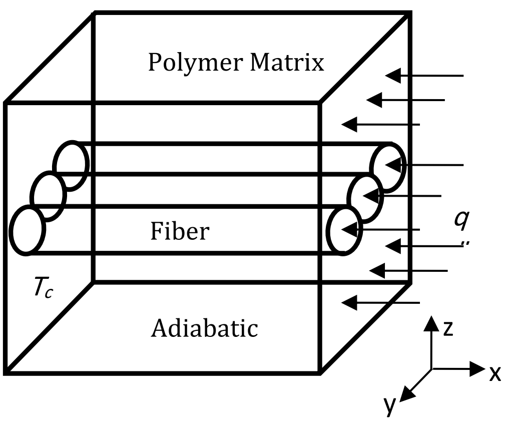

d) Triplet fibers along the way heat flux

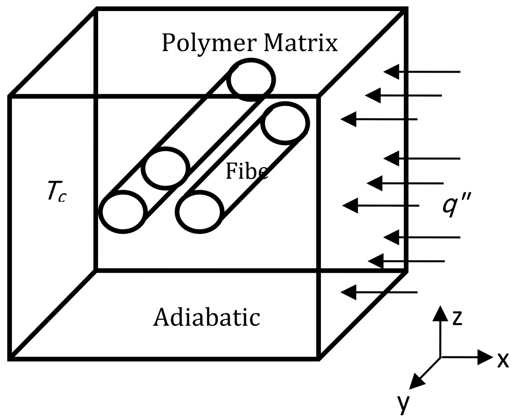

e) Triangular fibers perpendicular to heat flux

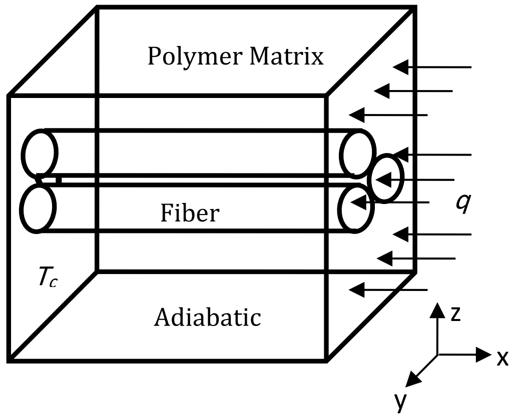

f) Triangular fibers along the way heat flux

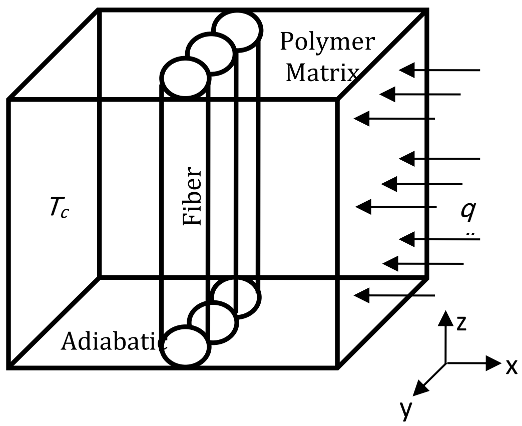

g) Triplet fibers perpendicular to the adiabatic wall

Fig. 1. Schematic diagrams of fibers and polymer matrix in a different arrangement

In this approach, the solid domain is made discrete in uniform Cartesian cells; each holds a fixed number of Distribution Functions (DF) that represent the number of solid particles moving in these discrete directions. Hence, depending on the dimension and number of thermal directions, different models can be used. In the LBM, integral distribution functions over boundaries must be integral and calculated. Therefore, suitable equations need for calculating distribution functions on boundaries for a given boundary condition. The present study examined 3D solid using a cubical lattice with seven temperature vectors for the temperature field.

Table 1. temperature vectors of the D3Q7 model

i	c_i
0	(0,0,0)
1	$(1,0,0)c$
2	$(-1,0,0)c$
3	$(0,-1,0)c$
4	$(0,1,0)c$
5	$(0,0,1)c$
6	$(0,0,-1)c$

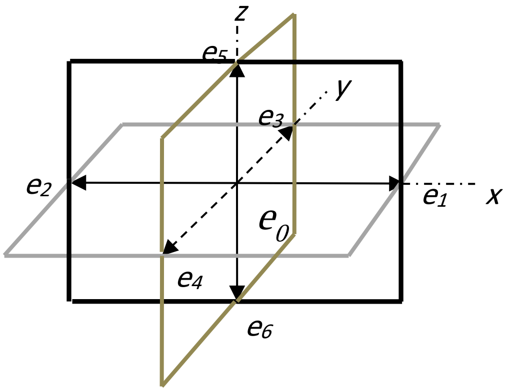

Fig. 2. Schematic diagrams of 3D temperature vectors at D3Q7 model

The temperature vectors $c_0, \ldots, c_6$ Of the D3Q7 model is shown in Fig. 2.

The LBM used the simplest algorithm to simulate the fluid flow and boundary conditions with good accuracy. Also, this method simultaneously analyzed data, post-processing, and evaluated them. For each temperature vector at the D3Q7 model, a particle DF is stored that presented in Table 1. where $c = \Delta x/\Delta t$ and k is the Lattice velocity direction. The LB model used in the present work is the same as that employed in [24]. The DFs are calculated by solving the Lattice Boltzmann Equation (LBE), a special discretization of the kinetic Boltzmann equation. The thermal Lattice Boltzmann equations [25] based on a uniform Lattice with Bhatnagar–Gross–Krook (BGK) collision model is represented in Eq. (2) [24]:

$$g_i(x + c_i\Delta t, t + \Delta t) - g_i(x,t) = -\frac{\Delta t}{\tau_c}\left(g_i(x,t) - g_i^{eq}(x,t)\right) \quad (2)$$

Where c_i is the Lattice velocity, while g_i is energy distribution functions. τ_c is the controlling factors of the rate equilibrium. The equilibrium energy distribution function for the current 3D application, based on the D3Q7 model, is expressed as [26]:

$$g_0^{eq} = \frac{T}{4}, \qquad g_{1-6}^{eq} = \frac{T}{8}, \quad (3)$$

The temperature vectors of the D3Q7 model are presented in Table 2.

Table 2. temperature vectors of the D3Q7 model [26]

i	ω_i
0	1/4
1	1/8
2	1/8
3	1/8
4	1/8
5	1/8
6	1/8

The temperature vectors of the D3Q7 model are presented in Table 2 [26].

$$T(x,t) = \sum_{i=0}^{6} g_i(x,t) \quad (4)$$

3.2. Validation for LBM

In this section, according to Fig. 3, the results of the simulation of conduction heat transfer are compared and verified in an environment with two solids with different conductivity coefficient k_1 and $k_2 = \frac{k_1}{2}$ [23].

According to Fig. 3, the conduction heat transfer relationship between two solid bodies are represented in Eq. (5):

$$k_1 \frac{(T' - T_c)}{\frac{L}{2}} = k_2 \frac{(T_h - T')}{\frac{L}{2}}$$
$$\rightarrow T' = \frac{T_h + \frac{k_1}{k_2}T_c}{\frac{k_1}{k_2} + 1} \quad (5)$$

The energy equation is expressed according to the physical condition of the problem is represented in Eq. (6):

$$\frac{\partial^2 T}{\partial y^2} = 0 \ , \quad \frac{\partial T}{\partial y} = C_1$$
$$\rightarrow T(y) = C_1 y + C_2 \quad (6)$$

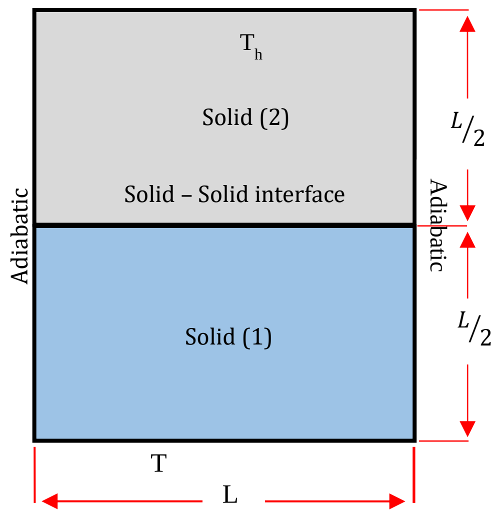

Fig. 3. Schematic of solid-solid hybrid heat transfer

For the first solid body with a conductivity coefficient k_1, the boundary conditions are represented in Eq. (7) and (8):

$$y = 0 \;\rightarrow\; T_c = C_2 \qquad (7)$$

$$y = 0 \;\rightarrow\; T_c = C_2 \qquad (8)$$

By inserting the Eq. (5) in the Eq. (8), so:

$$\frac{T_h + \frac{k_1}{k_2}T_c}{\frac{k_1}{k_2}+1} = \frac{C_1 L}{2} + T_c \;\rightarrow\; C_1 = \frac{2(T_h - T_c)}{L(\frac{k_1}{k_2}+1)} \qquad (9)$$

By replacing the Eqs. (7) and (8) instead of the constant coefficients C_1 and C_2 in Eq. (6), so:

$$T(y) = \frac{2(T_h - T_c)}{L(\frac{k_1}{k_2}+1)} y + T_c \qquad 0 \le y \le \frac{L}{2} \qquad (10)$$

For the second solid body with a conductivity coefficient k_2, the boundary conditions are represented in Eq. (11) and (12):

$$y = {}^{L}/_{2} \;\rightarrow\; T' = \frac{C_1 L}{2} + C_2 \qquad (11)$$

$$y = L \;\rightarrow\; T_h = C_1 L + C_2 \qquad (12)$$

Using the Eqs. (11) and (12), the constant coefficients C_1 and C_2 are represented in Eq. (13) and (14):

$$T_h - T' = \frac{C_1 L}{2} \;\rightarrow C_1 = \frac{2(T_h - T')}{L} \qquad (13)$$

$$2T' - T_h = C_2 \qquad (14)$$

By inserting the Eq. (5) in Eq. (13), the constant-coefficient C_1 is represented in Eq. (15):

$$C_1 = \frac{2}{L}\left(\frac{T_h\frac{k_1}{k_2} + T_h - T_h - \frac{k_1}{k_2}T_c}{\frac{k_1}{k_2}+1}\right) \qquad (15)$$

$$\rightarrow\; C_1 = \frac{2}{L}\frac{k_1}{k_2}\left(\frac{T_h - T_c}{\frac{k_1}{k_2}+1}\right)$$

By inserting the Eq. (5) in Eq. (14), the constant-coefficient C_2 is represented in Eq. (16):

$$C_2 = \frac{2T_h + 2\frac{k_1}{k_2}T_c - 2T_h\frac{k_1}{k_2} - 2T_h}{\frac{k_1}{k_2}+1} + T_h \qquad (16)$$

$$\rightarrow\; C_2 = -2\frac{k_1}{k_2}\left(\frac{T_h - T_c}{\frac{k_1}{k_2}+1}\right) + T_h$$

By inserting the Eqs. (15) and (16) in the Eq. (6), so:

$$T(y) = \frac{2(T_h - T_c)}{L\left(\frac{k_1}{k_2}+1\right)}(y - L) + T_c, \frac{L}{2} \le y \le L \qquad (17)$$

With compression of solving Eqs. (7) and (17) by the LBM and analytical solution. As shown in Fig. 4, there is good accuracy between the LBM and the analytical solution.

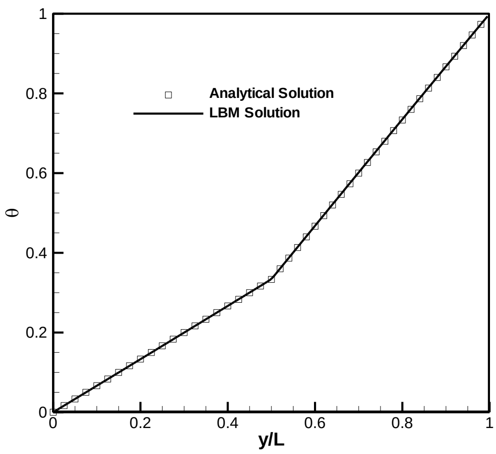

Fig. 4. Comparison between LBM and analytical solution

Here, θ is the nondimensional temperature that is equal to $(T - T_c/T_h - T_c)$.

4. Results and Discussion

In this research, the effects of different arrangements of 3D fibers on the thermal conductivity coefficient of PMC are presented under heat flux boundary conditions. Fig. 5 illustrates the nondimensional temperature field of PMC with the arrangement of a fiber perpendicular to heat flux and along the way heat flux at time steps 1000, 4000, 8000, 12000, 16000, and 20000. According to this Fig., nondimensional temperature field in a PMC with the arrangement of a fiber perpendicular to heat flux had a greater rate than a PMC with the arrangement of a fiber along the way heat flux. Nevertheless, Han et al. [13] increased the thermal conductivity of carbon fiber polymer matrix composite by curing pressure increase and filler incorporation. Also, Jan et al. [15] enhanced the thermal conductivity of carbon fiber polymer–matrix composites in the through-thickness direction by nano structuring the interlaminar interface with carbon black.

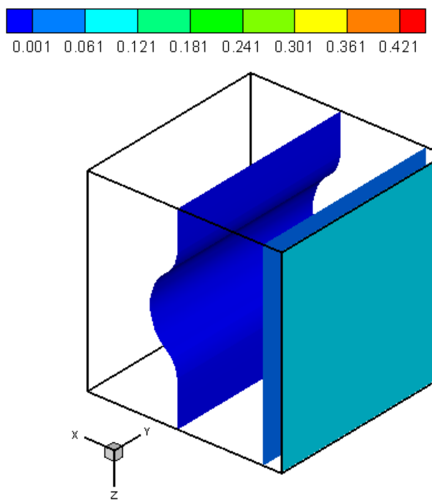

a) A fiber perpendicular to heat flux at *time step* = 1000

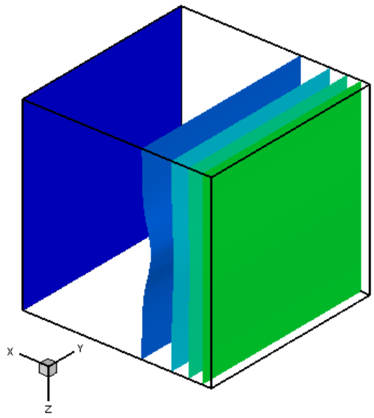

b) A fiber perpendicular to heat flux at $time\ step = 4000$

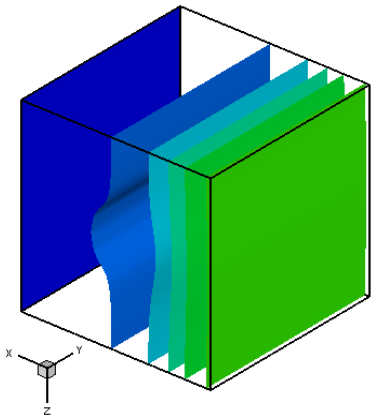

c) A fiber perpendicular to heat flux at $time\ step = 8000$

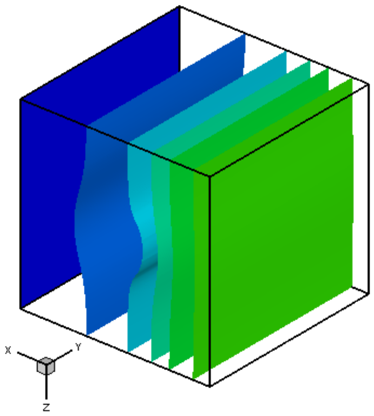

d) A fiber perpendicular to heat flux at $time\ step = 12000$

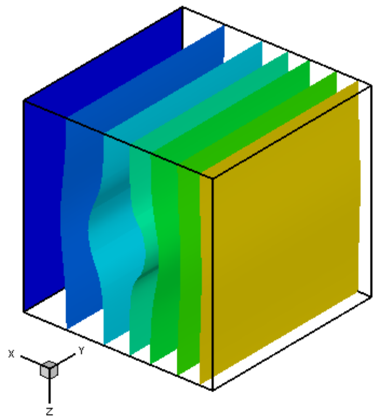

e) A fiber perpendicular to heat flux at $time\ step = 16000$

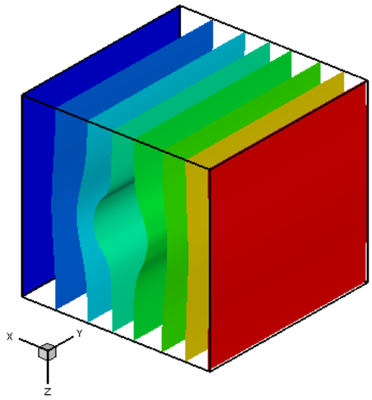

f) A fiber perpendicular to heat flux at $time\ step = 20000$

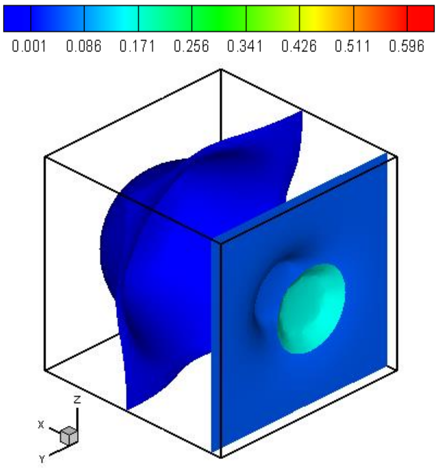

g) A fiber along the way heat flux at $time\ step = 1000$

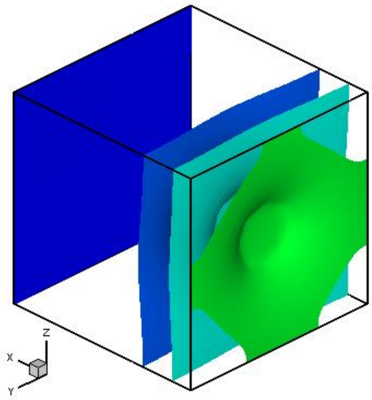

h) A fiber along the way heat flux at $time\ step = 4000$

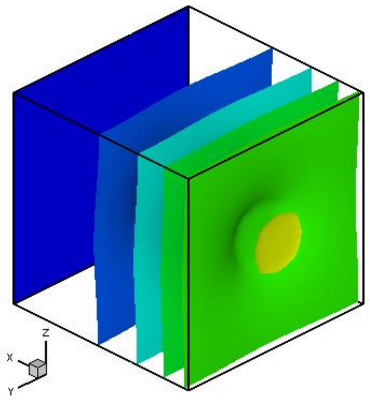

i) A fiber along the way heat flux at $time\ step = 8000$

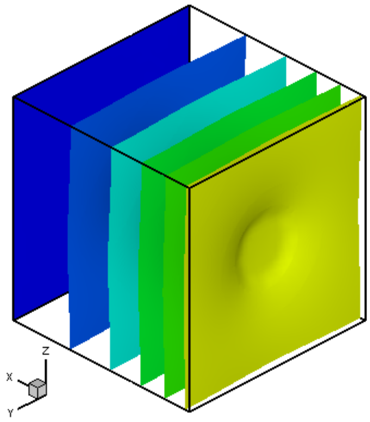

j) A fiber along the way heat flux at *time step* = 12000

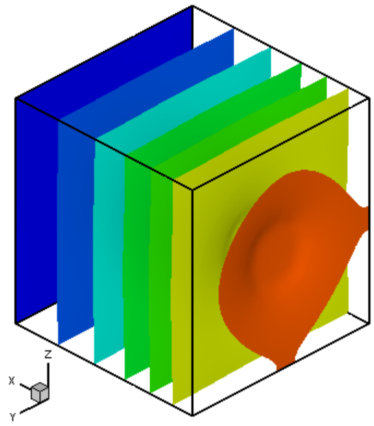

k) A fiber along the way heat flux at *time step* = 16000

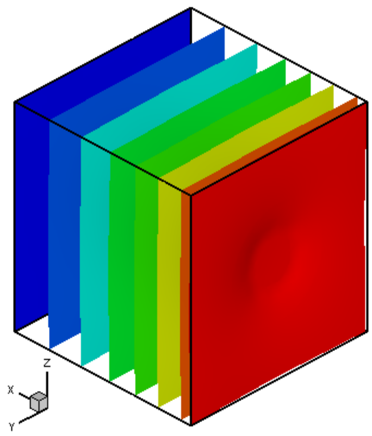

l) A fiber along the way heat flux at *time step* = 20000

Fig. 5. Comparison between nondimensional temperature field of PMC with the arrangement of a fiber perpendicular to heat flux and along the way heat flux

Fig. 6 illustrates the nondimensional temperature field of PMC with the arrangement of triplet fiber perpendicular to heat flux and along the way heat flux at time steps 1000, 4000, 8000, 12000, 16000, and 20000. According to this Fig., nondimensional temperature field in a PMC with the arrangement of triplet fiber perpendicular to heat flux had a greater rate than a PMC with the arrangement of triplet fiber along the way heat flux.

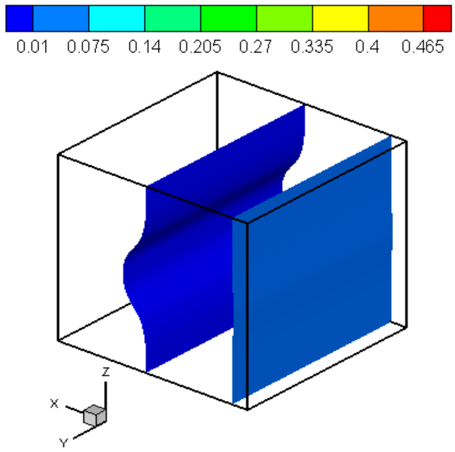

a) Triplet fiber perpendicular to heat flux at *time step* = 1000

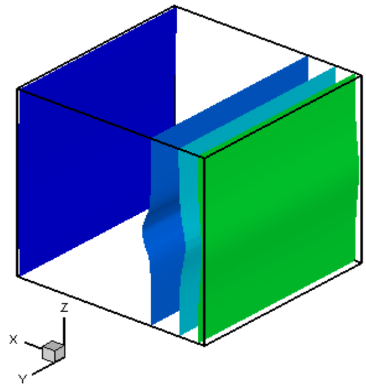

b) Triplet fiber perpendicular to heat flux at *time step* = 4000

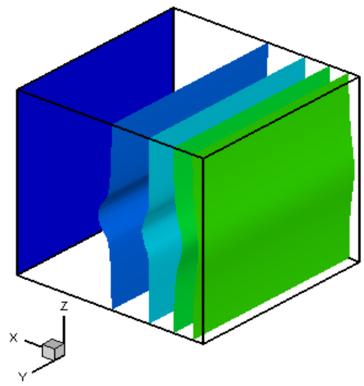

c) Triplet fiber perpendicular to heat flux at *time step* = 8000

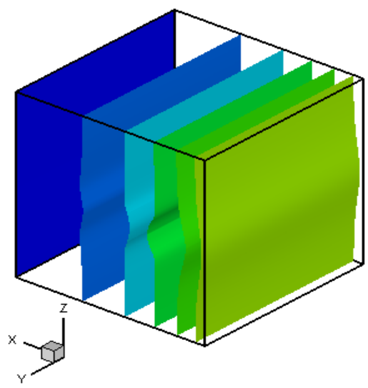

d) Triplet fiber perpendicular to heat flux at *time step* = 12000

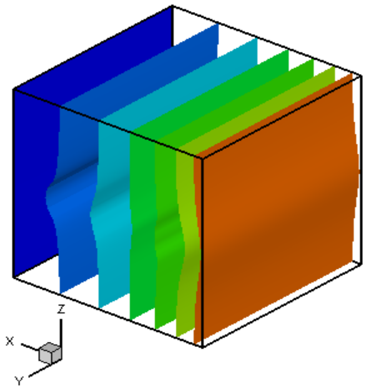

e) Triplet fiber perpendicular to heat flux at
$time\ step = 16000$

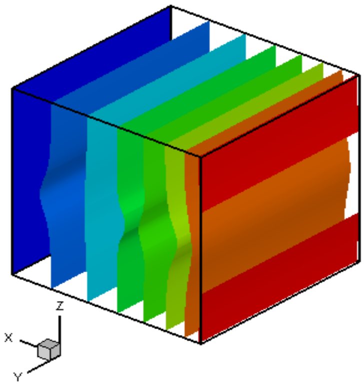

f) Triplet fiber perpendicular to heat flux at
$time\ step = 20000$

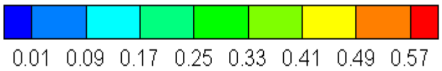

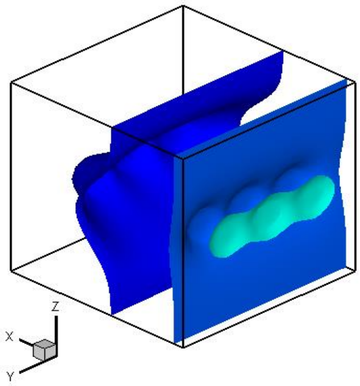

g) Triplet fiber along the way heat flux at
$time\ step = 1000$

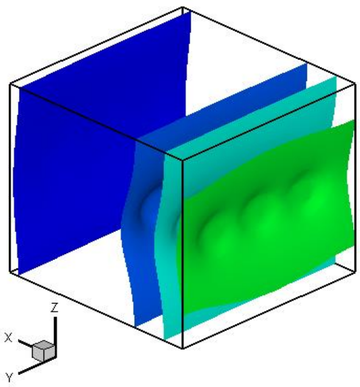

h) Triplet fiber along the way heat flux at
$time\ step = 4000$

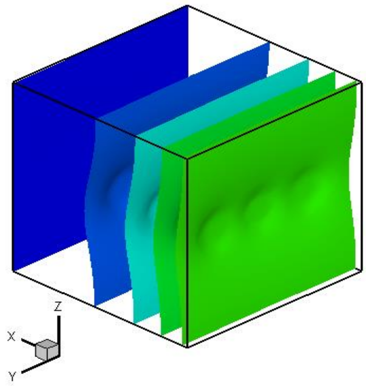

i) Triplet fiber along the way heat flux
at $time\ step = 8000$

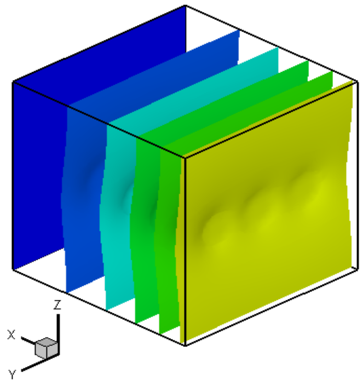

j) Triplet fiber along the way heat flux at
$time\ step = 12000$

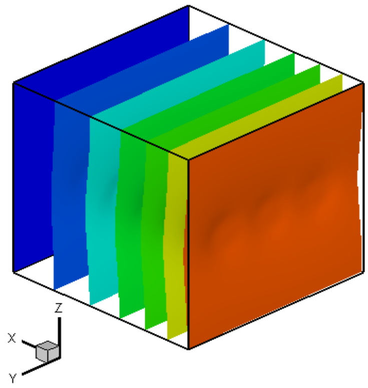

k) Triplet fiber along the way heat flux at
$time\ step = 16000$

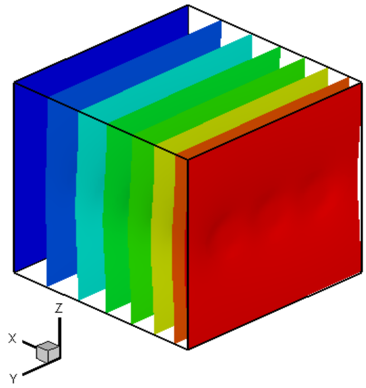

l) Triplet fiber along the way heat flux at
$time\ step = 20000$

Fig. 6. Comparison between nondimensional temperature field of PMC with arrangement of triplet fiber perpendicular to heat flux and along the way heat flux

Fig. 7 illustrates the nondimensional temperature field of PMC with the arrangement of triangular fiber perpendicular to heat flux and along the way heat flux at time steps 1000, 4000, 8000, 12000, 16000 20000. According to this Fig., nondimensional temperature field in a PMC with the arrangement of triangular fiber perpendicular to heat flux had a greater rate than a PMC with the arrangement of triangular fiber along the way heat flux.

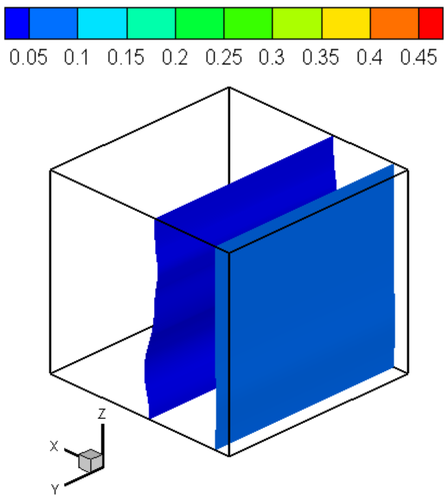

a) Triangular fiber perpendicular to heat flux at $time\ step = 1000$

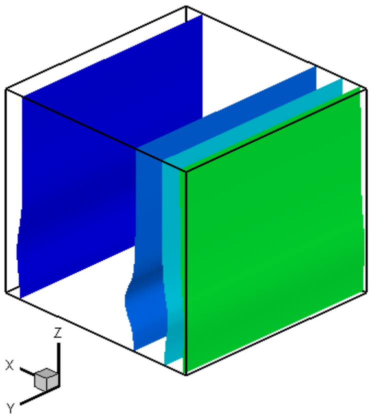

b) Triangular fiber perpendicular to heat flux at $time\ step = 4000$

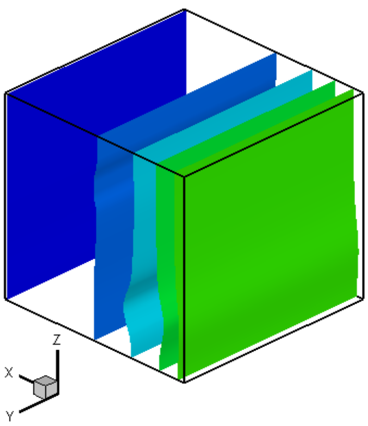

c) Triangular fiber perpendicular to heat flux at $time\ step = 8000$

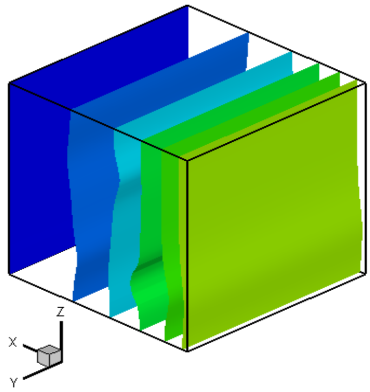

d) Triangular fiber perpendicular to heat flux at $time\ step = 12000$

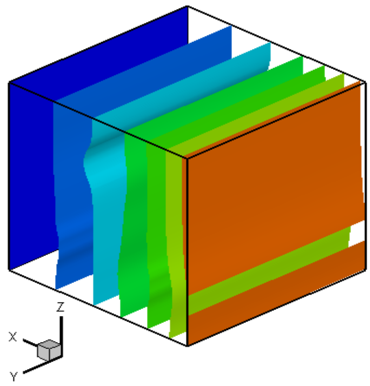

e) Triangular fiber perpendicular to heat flux at $time\ step = 16000$

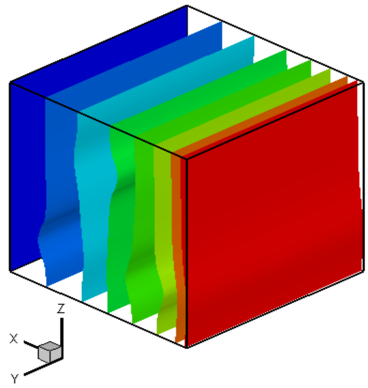

f) Triangular fiber perpendicular to heat flux at $time\ step = 20000$

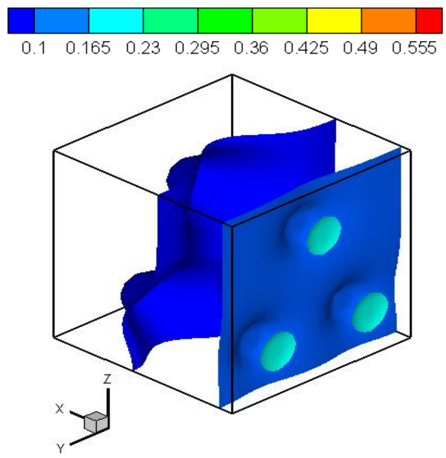

g) Triangular fiber along the way heat flux at $time\ step = 1000$

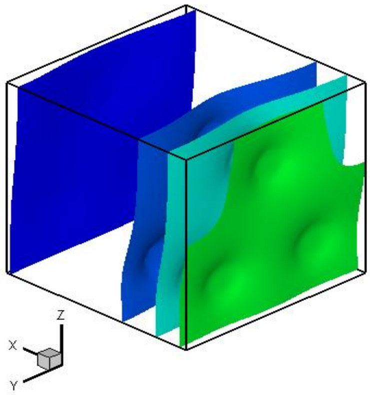

h) Triangular fiber along the way heat flux at $time\ step = 4000$

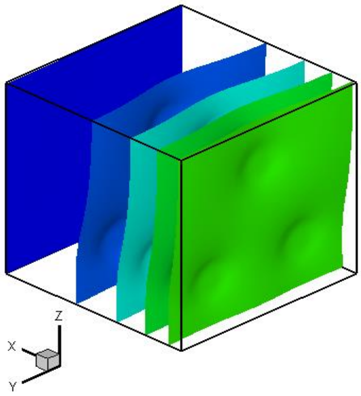

i) Triangular fiber perpendicular to heat flux at $time\ step = 8000$

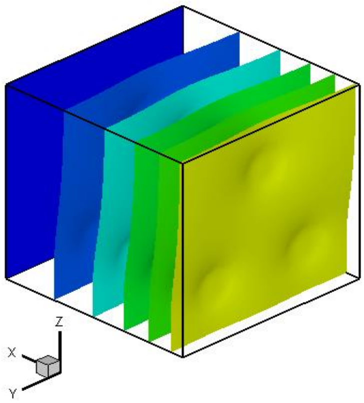

j) Triangular fiber along the way heat flux at $time\ step = 12000$

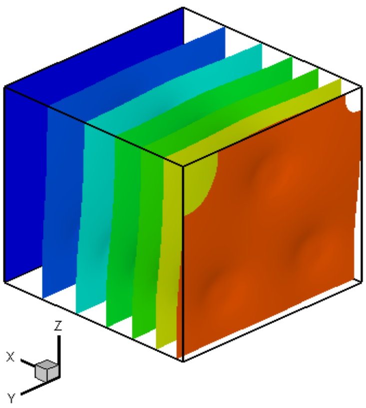

k) Triangular fiber along the way heat flux at $time\ step = 16000$

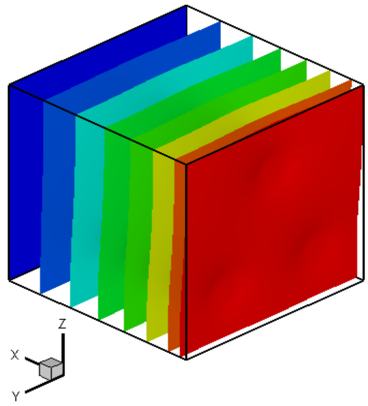

l) Triangular fiber along the way heat flux at $time\ step = 20000$

Fig. 7. Comparison between nondimensional temperature field of PMC with the arrangement of triplet fiber perpendicular to heat flux and along the way heat flux

Fig. 8 illustrates the nondimensional temperature field of PMC with the arrangement of triplet fiber perpendicular to the adiabatic wall at time steps 1000, 4000, 8000, 12000, 16000, and 20000. With the comparison of Figs. 8 and 6, nondimensional temperature field in a PMC with the arrangement of triplet fiber perpendicular to heat flux had a greater rate than a PMC with the arrangement of triplet fiber along the way the adiabatic wall.

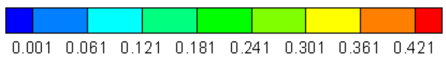

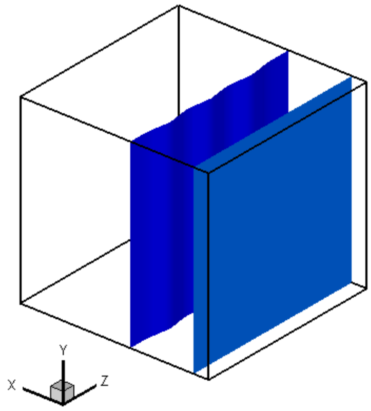

a) $time\ step = 1000$

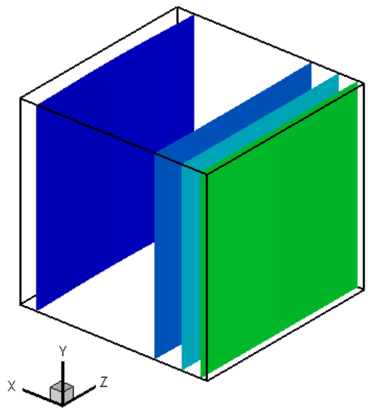

b) $time\ step = 4000$

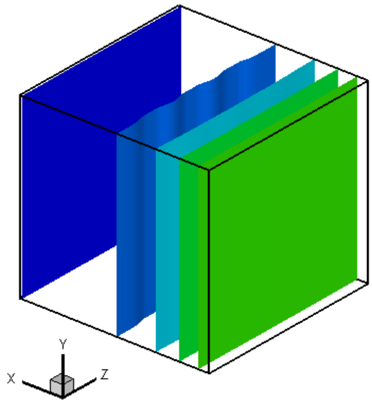

c) $time\ step = 8000$

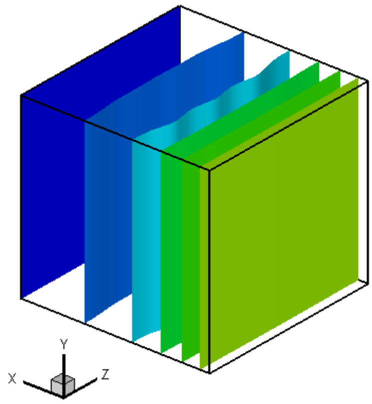

d) $time\ step = 12000$

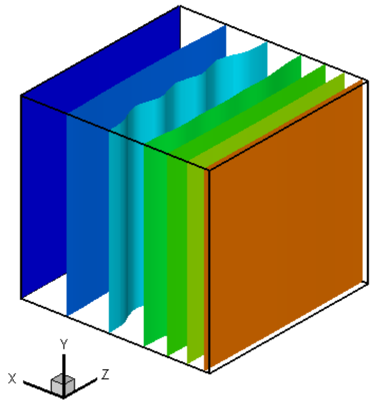

e) $time\ step = 16000$

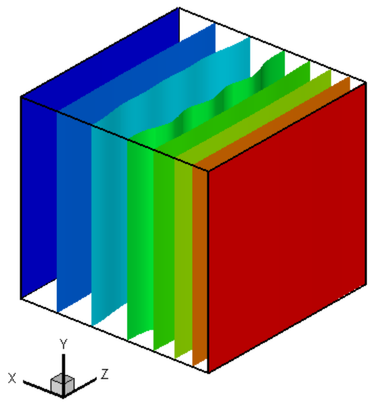

f) $time\ step = 20000$

Figure 8. Comparison nondimensional temperature field of PMC with the arrangement of triplet fibers perpendicular to the adiabatic wall at time steps 1000-20000

Fig. 9 illustrates the isothermal of PMC with a different arrangement of 3D fibers on thermal conductivity coefficient of PMC at time steps 1000, 4000, 8000, 12000, 16000, and 20000. According to this Fig., minimum isothermals were in PMCs with triplet and triangular fibers arrangement perpendicular to heat flux, respectively.

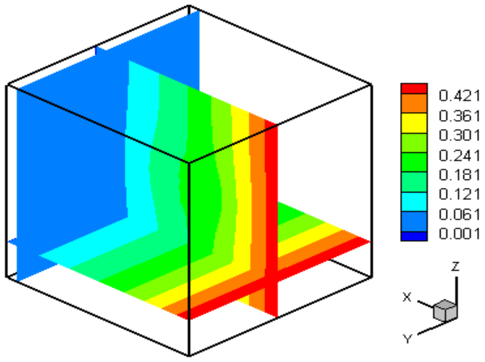

a) A fiber perpendicular to heat flux

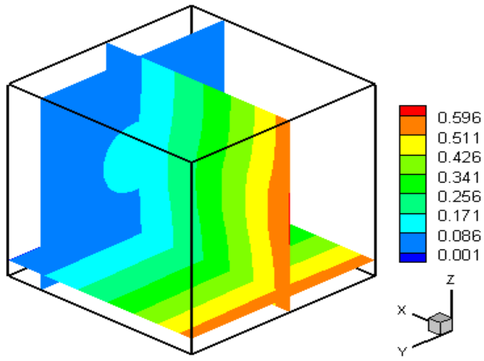

b) a fiber along the way heat flux

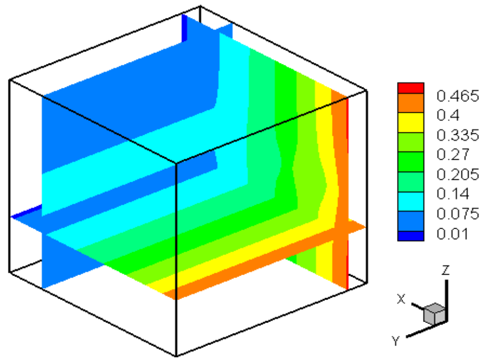

c) Triplet fibers perpendicular to heat flux

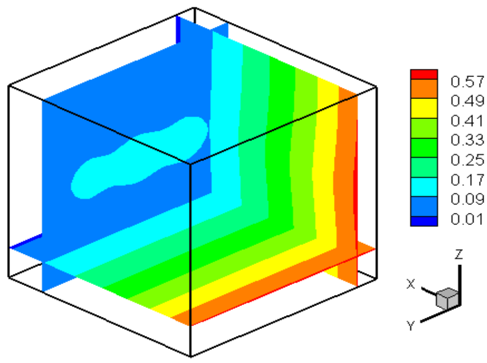

d) Triplet fibers along the way heat flux

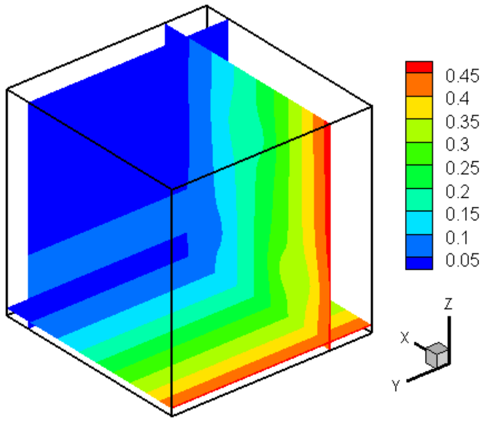

e) Triangular fibers perpendicular to heat flux

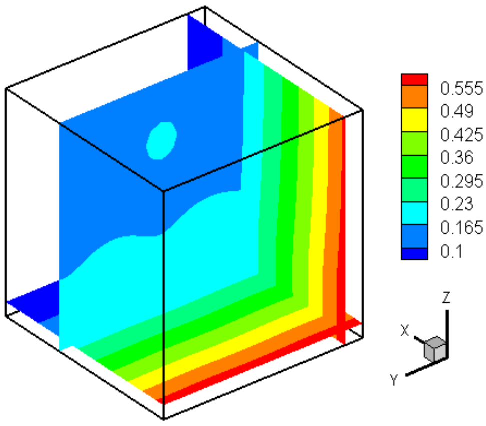

f) Triangular fibers along the way heat flux

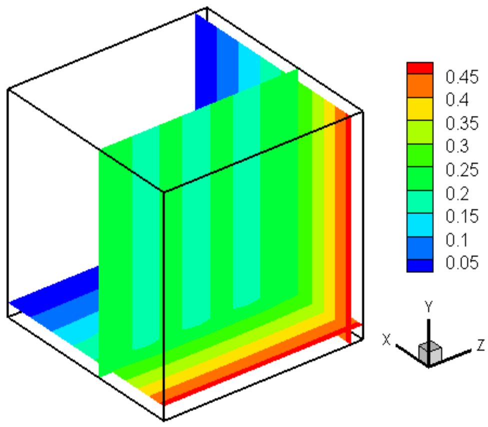

g) Triplet fibers perpendicular to the adiabatic wall

Fig. 9. Comparison between isothermal of PMC with the arrangement of a fiber

Fig. 10 illustrates nondimensional local temperature on the wall with heat flux boundary condition at y direction in PMCs with a different arrangement of 3D fibers. According to this Fig., the maximum of nondimensional local temperatures was $0.55 < \theta < 0.6$ in PMCs with the arrangement of a fiber, triplet, and triangular fibers along the way heat flux, respectively. Also, the minimum of nondimensional local temperatures was $0.44 < \theta < 0.48$ in PMCs with the arrangement of triplet, triangular fibers, and a fiber perpendicular to heat flux, respectively.

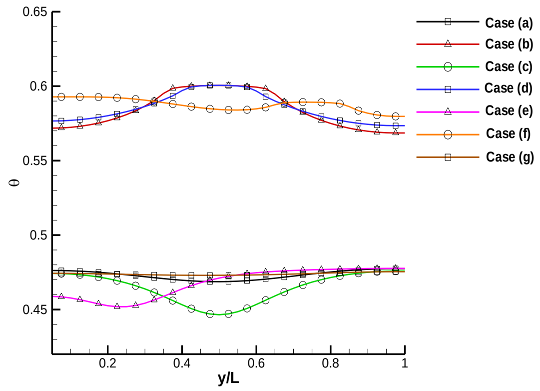

Fig. 10. The nondimensional local temperature on the wall with heat flux boundary condition at y direction

Fig. 11 illustrates nondimensional local temperature on the wall with heat flux boundary conditions at z direction in PMCs with a different arrangement of 3D fibers. Similar to Fig 10., the maximum of nondimensional local temperatures was $0.55 < \theta < 0.6$ in PMCs with the arrangement of a fiber, triplet, and triangular fibers along the way heat flux, respectively. Also, the minimum of nondimensional local temperature was $\theta \approx 0.445$ in a PMC with the arrangement of triplet fibers perpendicular to heat flux that is a fixed line.

Table 3 presents the nondimensional mean temperature on the wall with heat flux boundary condition of PMC with a different arrangement of 3D fibers. According to this table, maximum and minimum of nondimensional mean temperature were in PMCs with the arrangement of triangular and triplet fibers perpendicular to heat flux, respectively.

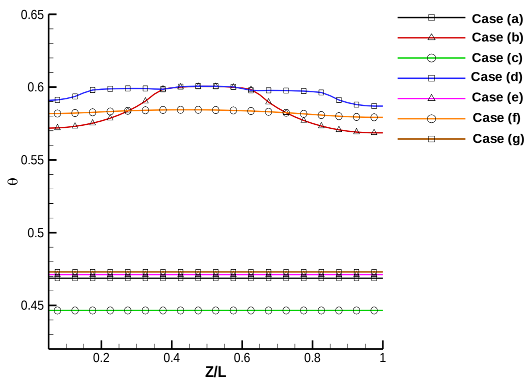

Fig. 11. The nondimensional local temperature on the wall with heat flux boundary condition at z direction

Table 3. Nondimensional mean temperature on the wall with heat flux boundary condition

Cases	θ
a	0.473
b	0.574
c	0.465
d	0.583
e	0.468
f	0.585
g	0.474

Table 4 presents the nondimensional thermal conductivity coefficient on the wall with heat flux boundary condition of a PMC with a different arrangement of 3D fibers into the thermal conductivity coefficient of the case (a). According to this table, maximum and minimum of nondimensional thermal conductivity coefficient were in PMC with the arrangement of triplet fibers perpendicular to heat flux and triangular fibers along the way heat flux, respectively.

Table 4. Nondimensional thermal conductivity coefficient on the wall with heat flux boundary condition

Cases	$k_x = k/k_{x,a}$
a	1
b	0.824
c	1.017
d	0.811
e	1.011
f	0.809
g	0.999

5. Conclusions

In this paper, the effects of different arrangements of 3D fibers on the thermal conductivity coefficient of PMC were investigated under heat flux boundary conditions. The D3Q7 LB method was used to solve nondimensional temperature fields, isothermal, isothermal, nondimensional thermal conductivity coefficient, nondimensional mean, and local temperature in 7 cases of PMCs. Finally, some of the main points summarized:

- Nondimensional temperature field in a PMC with the arrangement of a fiber, triplet, and triangular perpendicular to heat flux had a greater rate than a PMC with the arrangement of fibers along the way heat flux.
- Maximum and minimum of nondimensional mean temperature were in PMCs with the arrangement of triangular and triplet fibers perpendicular to heat flux, respectively.
- Maximum and minimum of nondimensional thermal conductivity coefficient were in PMC with the arrangement of triplet fibers perpendicular to heat flux, $(k_{x,c} = 1.017)$ and triangular fibers along the way heat flux, $(k_{x,f} = 0.809)$, respectively.

Nomenclature

k_b	Boltzmann constant
C_i	lattice velocity
k	thermal conductivity coefficient (W/m. K)
k_x	nondimensional thermal conductivity coefficient
ω_i	lattice grade weight
x, y, z	coordinates (m)
L	dimensions of enclosure (m)
g_i	particle energy distribution function
g_i^{eq}	equilibrium particle energy distribution function
q''	heat flux (W/m^2)
T_c	the temperature of the cold wall (K)
α	thermal diffusivity (m^2/s)
β	thermal expansion (1/K)
τ_c	relaxation time relating to temperature field
θ	nondimensional temperature $((T - Tc)/(T_h - T_c))$

References

[1] Peiravi, M. M., Alinejad, J., Domiri Ganji, D., and Maddah, S., 2019. Numerical study of fins arrangement and nanofluids effects on three-dimensional natural convection in the cubical enclosure. *Transp phenom nano micro scales*, 7(2), pp. 97-112.

[2] Peiravi, M. M., and Alinejad, J., 2019. Hybrid conduction, convection, and radiation heat transfer simulation in a channel with rectangular cylinder. *Journal of thermal analysis and calorimetry*, 140, pp. 2733-2747.

[3] Peiravi, M. M., Alinejad, J., Domiri Ganji, D., and Maddah, S., 2019. 3D optimization of baffle arrangement in a multi-phase nanofluid natural convection based on numerical simulation. *International journal of numerical methods for heat and fluid flow*, 30, pp. 2583-2605.

[4] Peiravi, M. M., and Alinejad, J., 2021. Nano particles distribution characteristics in multi-phase heat transfer between 3D cubical enclosures mounted obstacles. *Alexandria engineering journal*, 60(6), pp. 5025-5038.

[5] Alinejad, J., and Peiravi, M. M., 2020. Numerical analysis of secondary droplets characteristics due to drop impacting on 3d cylinders considering dynamic contact angle. *Meccanica*, 55(10), pp. 1975–2002.

[6] MaL, Y., Li, B., Gao, G. X., Yang, X. Y., and You, Y., 2016. Effect of Montmorillonite On the Ionic Conductivity and Electrochemical Properties of a Composite Solid Polymer Electrolyte Based On Poly vinylidenedi fluoride/Polyvinyl Alcohol Matrix for

Lithium Ion Batteries. *Journal of Electrochimica acta,* 187(1), pp. 535-542.
[7] Vite-Torres, J., Vite-Torres, M., Laguna-Camacho, J. R., Escalante-Martínez, J. E., Gallardo-Hernández, E. A., and Vera-Cardenas, E. E., 2014. Wet Abrasive Behavior of Composite Materials Obtained from Solid Residuals Mixed with Polymer and Ceramic Matrix. *Ceramics international,* 40(7), pp. 9345-9353.
[8] Sari-Bey, S., Fois, M., Krupa, I., Ibos, L., Benyoucef, B., and Candau, Y., 2014. Thermal Characterization of Polymer Matrix Composites Containing Microencapsulated Paraffin in Solid or Liquid State. *Energy Conversion and Management,* 78(1), pp. 796-804.
[9] Ivosevic, M., Knight, R., Kalidindi, S. R., Palmese, G. R., and Sutter, J. K., 2006. Solid Particle Erosion Resistance of Thermally Sprayed Functionally Graded Coatings for Polymer Matrix Composites. *Surface and Coatings Technology,* 200(16), pp. 5145-5151.
[10] Cenna, A. A., Doyle, J., Page, N. W., Beehag, A., and Dastoor, P., 2000. Wear Mechanisms in Polymer Matrix Composites Abraded by Bulk Solids. *Wear,* 240(1), pp. 207-214.
[11] Roy, M., Vishwanathan, B., and Sundararajan, G., 1994. The Solid Particle Erosion of Polymer Matrix Composites. *Wear,* 171(1), pp. 149-161.
[12] Shemelya, C., De La Rosa, A., Torrado, A. R., Yu, K., Domanowski, J., Bonacuse, P. J., Martin, R. E., Juhasz, M., Hurwitz, F., Wicker, R. B., Conner, B., MacDonald, E., and Roberson, D. A., 2017. Anisotropy of Thermal Conductivity in 3D Printed Polymer Matrix Composites for Space Based Cube Satellites. *Additive Manufacturing,* 16(1), pp. 186-196.
[13] Han, S., Chung, and D. D. L., 2011. Increasing The Through Thickness Thermal Conductivity of Carbon Fiber Polymer Matrix Composite by Curing Pressure Increase and Filler Incorporation. *Composites Science and Technology,* 71(16), pp. 1944-1952.
[14] Kim, W. J., Taya, M., and Nguyen, M. N., 2019. Electrical and Thermal Conductivities of a Silver Flake/Thermosetting Polymer Matrix Composite. *Mechanics of Materials,* 41(10), pp. 1116-1124.
[15] Jan, S. H., Yamada, T. L. Y., and Chung, D. D. L., 2015. Enhancing The Thermal Conductivity and Compressive Modulus of Carbon Fiber Polymer–Matrix Composites in The Through-Thickness Direction by Nano structuring the Inter laminar Interface with Carbon Black. *Carbon,* 46(7), pp. 1060-1071.
[16] Alva, G., Lin, Y., and Fang, G., 2021. Thermal and Electrical Characterization of Polymer/Ceramic Composites with Polyvinyl Butyral Matrix. *Materials Chemistry and Physics,* 205(3), pp. 401-415.
[17] Wang, Y., and Zhupanska, O. I., 2020. Modeling of Thermal Response and Ablation in Laminated Glass Fiber Reinforced Polymer Matrix Composites Due to Lightning Strike. *Applied Mathematical Modelling,* 53(6), pp. 118-131.
[18] Ghasemi, A. R., and Moradi, M., 2018. Effect of Thermal Cycling and Open-Hole Size On Mechanical Properties of Polymer Matrix Composites. *Polymer Testing,* 59(6), pp. 20-28.
[19] Yu, G. C., Wu, L. Z., Feng, L. J., and Yang, W., 2017. Thermal and Mechanical Properties of Carbon Fiber Polymer-Matrix Composites with A 3D Thermal Conductive Pathway. *Composite Structures,* 149(1), pp. 213-219.
[20] Takenaka, K., Ichigo, M., 2017. Thermal Expansion Adjustable Polymer Matrix Composites with Giant Negative Thermal Expansion Filler. *Composites Science and Technology,* 104(2), pp. 47-51.
[21] Chen, J., and Gao, X., 2017. Thermal and Electrical Anisotropy of Polymer Matrix Composite Materials Reinforced with Graphene Nanoplatelets and Aluminum-Based Particles. *Diamond and Related Materials,* 100(3), pp. 107571.
[22] Ouyang, Y., Ding, F., Bai, L. Li, X., Hou, G., Fan, J., and Yuan, F., 2017. Design of Network Al_2O_3 Spheres for Significantly Enhanced Thermal Conductivity of Polymer Composites. *Composites Part A: Applied Science and Manufacturing,* 128(1), pp. 105673.
[23] Wang, W., Ma, X., Sun, D., Qi, X., Yang, J., and Wang, Y., 2020. Achieving electrical insulation, high thermal conductivity and high fracture toughness in polyamide 6/carbon nanofiber composites through the interfacial welding effect of elastomer. *Composites part A: applied science and manufacturing*, 128(1), 105671.
[24] Mezrhab, A., Jami, M., Abid, C., Bouzidi, M., and Lallemand, P., 2006. Lattice Boltzmann modeling of natural convection in an inclined square enclosure with partitions attached to its cold wall. *International journal of heat and fluid flow*, 27(3), pp. 456–465.
[25] Peng, Y., Shu, C., and Chew, Y. T., 2003. Simplified thermal lattice Boltzmann model for incompressible thermal flows. *Physical review*, 68(2), pp. 1-8.
[26] Cheng, X., Su, R., Shen, X., Deng, T., Zhang, D., Chang, D., Zhang, B., and Qiu, Sh., 2020. Modeling of indoor airflow around thermal manikins by multiple-relaxation-time lattice

Boltzmann method with LES approaches. Numerical heat transfer applications, 77(2), pp. 215–231.

[27] Shigang, A., Rujie, H., and Yongmao, P., 2015. A Numerical Study on the Thermal Conductivity of 3D Woven C/C Composites at High Temperature. *Applied Composite Materials*, 22, pp. 823–835.

[28] Lu, Z., Yuan, Z., and Liu, Q., 2014. 3D numerical simulation for the elastic properties of random fiber composites with a wide range of fiber aspect ratios. *Computational Materials Science*, 90, pp. 123-129.

[29] Höller, J., Niedermeyer, J., Redenbach, C., Ecke, N., Schlarb, A. K., Andrä,H., and Klein, P., 2020. The effective thermal conductivity of double-reinforced composites. *Heat and Mass Transfer*, 56, pp. 2847–2857.

[30] Karkri, M., Aadmi, M., and El Hammouti, M., 2016. A numerical and experimental study on the effective thermal conductivity of conductive hollow tube composite. *Journal of Thermoplastic Composite Materials*, 29(10), pp. 1369-1391.

[31] Chai, Y., Liang, Sh., Zhou, Y., Lin, L., and Fu, F., 2019. 3D Microscale Heat Transfer Model of the Thermal Properties of Wood-Metal Functional Composites Based on the Microstructure. *Materials,* 12(17).

[32] Karkri, M., Ibos, L., and Garnier, B., 2015. Comparison of experimental and simulated effective thermal conductivity of polymer matrix filled with metallic spheres: Thermal contact resistance and particle size effect. *Journal of Composite Materials,* 49(24), PP. 3017-3030.

[33] Ejeh, C. J., Barsoum, I., Chizindu, G. O., Kodie, G. M., and Anachuna, J. I., 2020. Thermo-elastic behaviour of carbon-fiber reinforced polymer and the effect of adding nanoparticles at elevated heat intensity. *Heliyon,* 6(3), p.e03622.